THE VALUE OF MULTI-COMPONENT TEM DATA FOR THE ESTIMATION OF UXO TARGET PARAMETERS

Donald D. Snyder, Snyder Geoscience, Inc., Grand Junction, CO
Scott C. MacInnes, Zonge Engineering & Research Org., Inc, Tucson, AZ
Jennifer L. Hare, Zonge Engineering & Research Org., Inc, Tucson, AZ
Robert E. Grimm, Southwest Research Institute, Boulder, CO
Mary Poulton, University of Arizona, Tucson, AZ
Anna Szidarovszky, University of Arizona, Tucson, AZ

Abstract

Two multi-component multi-gate data sets from the Naval Research Laboratory's Baseline Ordnance Classification Test Site at Blossom Point, one acquired statically with a Geonics EM61-3D-3C and the other acquired dynamically with a Zonge NanoTEM system (DNT), are analyzed to determine the relative classification performance of the two systems. Not surprisingly, our classification performance is better with 3-component static data than it is with the 3-component dynamic data. Confirming published work by Grimm [4], classification is significantly improved when it is applied to the 3-component static data than when it is applied to a decimated data set consisting of only a single (z) component. However, early analyses of the dynamic data indicated that horizontal components provide marginal, if any, improvements in classification. Noise analyses of data from the two systems show that noise levels in the EM61-3D data set are approximately 40dB lower than those in the DNT system and that noise levels in the horizontal components at late times are 2-5 times higher in the vertical component. Noise reduction in statically acquired data can be attributed to stacking (~20dB) and the elimination of microphonic noise from antenna cart movements. With dynamically acquired data, the higher noise levels in the horizontal components together with uncertainties in antenna position and attitude are most likely the reason that the horizontal components do not unequivocally improve classification performance in the dynamic data.

Introduction

Recently published numerical model studies [1-3] and precision static measurements [4] conclusively demonstrate that target classification noticeably improves when physics-based target analysis is applied to multi-component multi-gate TEM data. The obvious explanation for the improvement is that the added independent information provided by the addition of the transients from the horizontal receiver antennas produces a more robust solution to the anisotropic dipole model that is widely used for target parameterization. But these conclusions are not as clear when using dynamic multi-axis multi-gate data from the same target set [5].

Confusion arises from analyses of static multi-component data acquired at the Naval Research Laboratories Blossom Point facility with the Geonics EM61-3D and dynamic multi-component data acquired with the Zonge DNT system. Major differences in the two systems include a 1 decade shift in the time-bandwidth, and the position and attitude errors that are inevitably associated with dynamically acquired data.[1] A third and perhaps most important difference arises from the fact that static measurements permit a substantial noise reduction through synchronous stacking. Static measurements over a period of 15-30 seconds can reduce noise levels by 15 dB or more over that observed in the dynamic data.

[1] As deployed at Blossom Point, the time bandwidth of the EM61-3D was $350 \le t \le 27900$ μs reported as 20 time gate values. The time bandwidth of the Zonge DNT system at Blossom Point was $1 \le t \le 1920$ μs reported as 31 time gates.

The availability of these two data sets, one acquired in the static mode and one acquired dynamically, provides with a rare opportunity to compare interpretations derived from similar, if not identical, processing and classification software. Moreover, the two data sets provide an opportunity to compare the performance of multi-component multi-gate data for UXO classification from the two methods of deployment. In this paper, we first present the two data sets and discuss briefly, two important sources of noise: position, and EMI. The balance of the paper is devoted to comparing the relative performance of each data set as measured by discrimination receiver operating characteristics (ROC) curves.

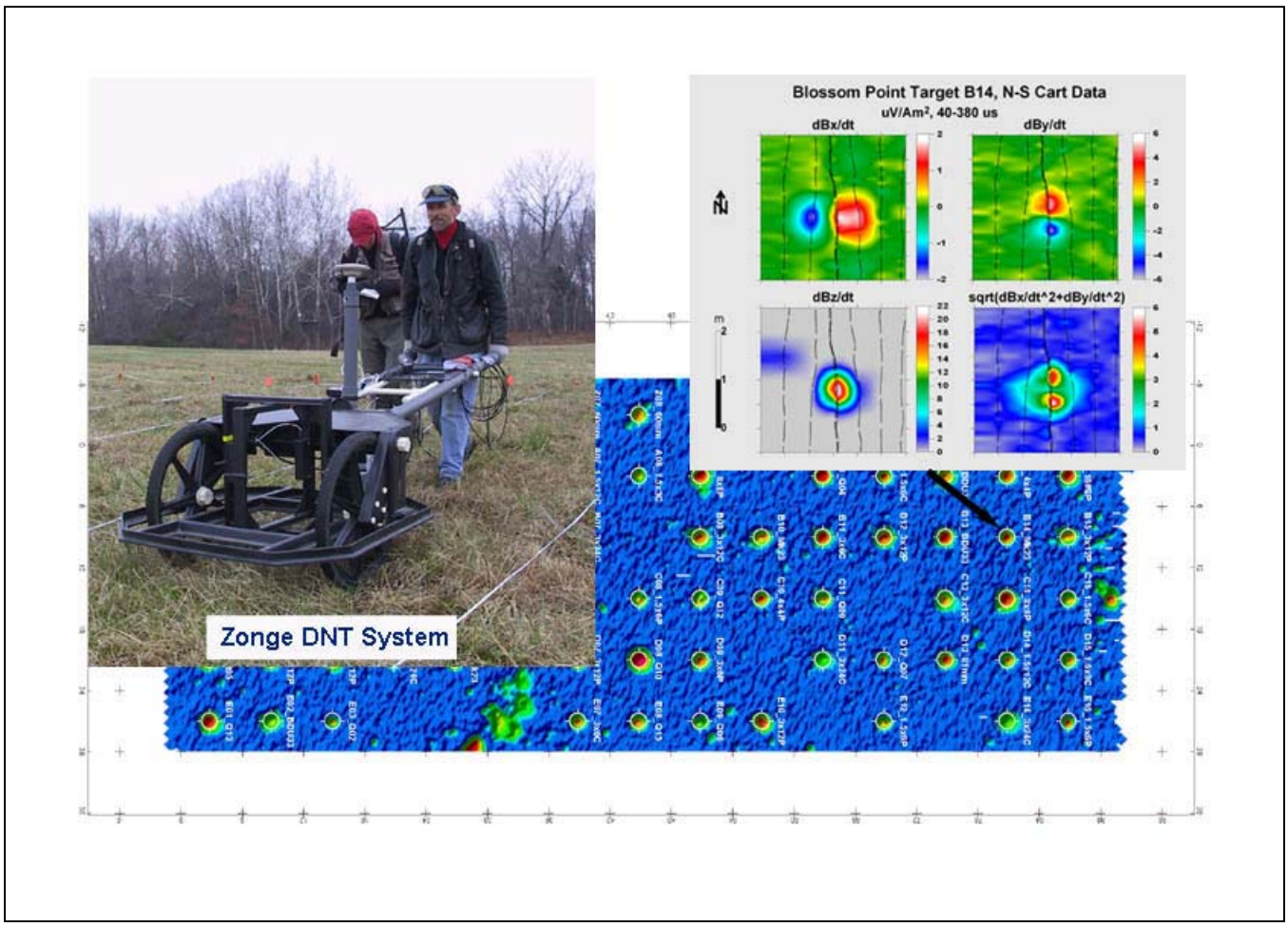

Figure 1: Composite figure showing the Zonge 4D DNT system in operation at Blossom point together with maps of the response from a composite gate from the vertical transient. The detailed map for target B14 shows three components. The maps have been generated from the N-S grid data.

The Blossom Point Data Sets

NLR's Baseline Ordnance Classification Test Site [6] is located at the Army's Blossom Point southeast of Washington. The test site includes a variety of inert ordnance (e.g., 60mm & 80mm mortars, Mk23 Practice Bombs), simulated ordnance (e.g., steel cyclinders), and clutter items emplaced in a grid on 6m centers and covering an area of approximately 90m x 36m (0.32ha/0.79 acre).

DNT-4D Data Set

Zonge Engineering surveyed Blossom Point in December, 2001 as a preliminary demonstration survey in connection with an ESTCP funded project to demonstrate its multi-gate (31) multi-component (3) TEM system. Two grids were acquired:

1. N-S Grid: Acquired at ½-m lane intervals.
2. E-W Grid: Acquired at 1-m lane intervals.

Figure 1 is a composite of a map with a color map of the vertical component response from a composite gate (gates 13-21) of the N-S DNT data together with a photo of the Zonge DNT antenna cart. In analyses that we show later in this paper, we present classification results based on the N-S grid and a composite of the N-S + E-W grids. The purpose of using the composite grid was to determine whether the additional data density over the targets provided by including the two grids during the model-based parameterization noticeably improved the quality of our classification.

Position Noise – During the survey, sensor position was recorded with a Leica SR530 RTK GPS system. Based on a statistical analysis of positions of the anomaly peak for our calibration target, a target over which we traversed many times each day, we have determined that our dynamic positions have a standard deviation of approximately 10cm [5].

Background EMI – We have compiled the statistics of each of the 31 time channels for all stations not falling within a radius of 1.5m of a target position in order to get an estimate of the RMS noise for each channel. The results of this analysis are shown in Figure 2. We have plotted results for both N-S and E-W data grids. We have labeled each of the curves according to the geographic orientation of the receiver antenna. Note that the noise levels are channel-specific and independent of the cart orientation. When the cart is oriented N-S, one of the antennas (say channel 1) is oriented along the X (E-W) axis, while the other antenna (channel 2) is oriented in the Y (N-S) direction. When the cart is oriented E-W, the roles of channel 1 and channel 2 will be reversed. In this noise plot, we see that the noise levels are a function of the receiver channel and are not effected by the direction in which the cart is pointing. In the Zonge GDP-32^{II}, the window widths increase directly with time. We expect, therefore, that when noise is random and uncorrelated, the TEM channel noise will decrease inversely with time (i.e. $\sim 1/\sqrt{t}$) as indeed it does in both the green and blue curves. The first 6 channels are comprised of a single A/D sample and therefore there is little or no attenuation of noise. It is expected that the noise levels as measured in the vertical (z) channel will be lower than the noise levels observed in the horizontal channels. And so one can rationalize the difference between the green and blue curves in Figure 2. The behavior of the red and green curves, however, is specific to their respective hardware channels. This suggests that at Blossom Point, the difference in the noise levels in the horizontal channels may arise from within the instrument itself. Moreover, the noise related to the channel represented by the red curves (hardware channel 2) does not decrease with the characteristic ($1/\sqrt{t}$) behavior, suggesting that this channel is picking up significant coherent noise.

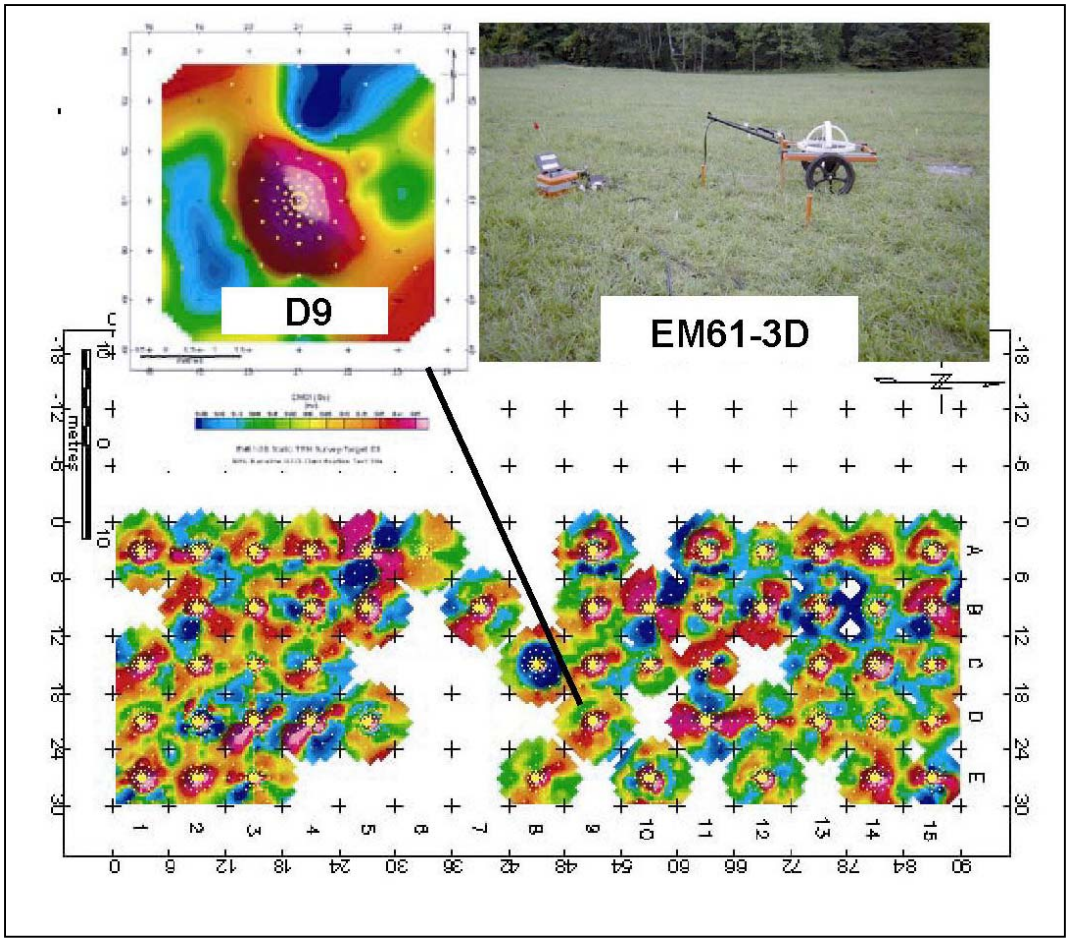

Figure 3: Composite figure showing the Geonics EM61-3D in operation at Blossom Point. The maps are color maps of all the targets measured together with a detailed map

EM61-3D-3C Data Set

Three-component multi-gate static TEM data were acquired with a Geonics EM61-3D-3C over 61 targets located in the main grid area at Blossom Point. Data over an additional 9 targets located over a number of small targets (20mm, 30mm, and 50 cal projectiles) located west of the main test area. Data were acquired at each of 74 discrete measurement points comprising a local template or measurement grid that was centered over the target. At each of the stations, data were integrated for 15s. All data were acquired using a base frequency of 7.5Hz for the transmitter waveform. We show in Figure 3, a composite figure with color mini-maps of the 61 targets in their correct spatial context, a detailed color map of one of the mini-maps showing the 74 measurement points, and a photograph of the Geonics equipment used to acquire the data.

Position Error-The EM61-3D data were acquired at static positions measured on a string grid. The cart was carefully positioned over each local grid point to within a few centimeters. Therefore, the position errors are 3 or 4 times smaller than those for the DNT data set.

EMI Noise – We estimated the noise level for each of the 20 EM61-3D channels using transient data from the outer ring (2.7m radius) of each of the 61 targets analyzed by Grimm. Figure 4 shows the RMS average error at each of the 20 time gates resulting from that analysis. The noise levels in the first 11 gates (t< 3ms) are approximately the same and fall off linearly with the log of window time (~ $1/\sqrt{t}$) reflecting the an increase in window width proportional to window time. However, after this point, the noise in the horizontal components (red and green) becomes distinctly higher than that of the vertical component (blue). In the last time gate, the noise level in dBx/dt is 2 times higher than that of dBz/dt. The noise level in dBy/dt is 3.4 times higher. The departure of all three curves from the $1/\sqrt{t}$ fall-off behavior at late time, particularly in the horizontal components, suggests that there may be either coherent noise or, perhaps, audio frequency natural noise (i.e., spherics) in the horizontal fields that is strongest in the NS (y) direction. Longer and/or tapered stacks may help reduce this coherent noise. Unlike Zonge's 3-channel NanoTEM receiver, the Geonics Protem 47D receiver used with the EM61-3D is a single channel receiver. Therefore, the difference in the noise levels at late times probably reflects coherent background EMI at Blossom Point and not instrument noise.

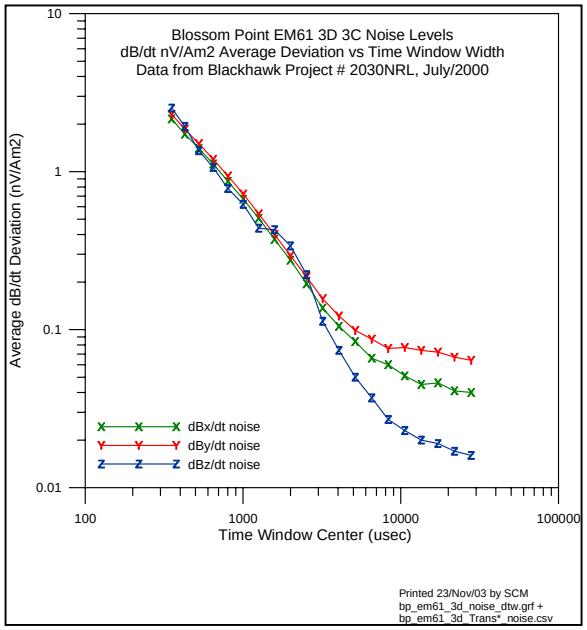

Figure 4: Channel noise estimates for the EM61-3D at Blossom Point.

Interpretation of Results

In the remainder of this paper, we compare results obtained by processing the two aforementioned data sets acquired at Blossom Point. Only the EM61-3D data have been processed by both the Blackhawk GeoServices organization [4] and the Zonge organization. To compare the efficacy of the horizontal components, we have decimated the original data sets to yield data sets containing only the transients for the vertical field (dBz/dt). To study the effect of greater density, we have combined the NS & EW DNT data grids to provide us with a data consisting of orthogonal profiles. Our interest in the use of orthogonal grids stems from statements by Nelson and others [7] that their model-based parameterization and, ultimately, their classifications were significantly improved by using data sets comprised of orthogonal profiles. We have tabulated the abbreviations that we use for the various data sets in Table 1. Unless otherwise noted, all parameters have been generated by the application of Zonge's dipole parameterization software (DNTDipole) on the indicated data set. The data set EM61_3D-XYZ_Grimm consists of the set of dipole parameters that were generated by Grimm.

Table 1: Abbreviations and explanations for the data sets used.

Data Set	Explanation
DNT_NS_EW_XYZ	3-Component DNT data - Combined NS & EW grids
DNT_NS_EW_Z	Single-component (z) DNT data - Combined NS&EW grids
DNT_NS_XYZ	3-Component DNT data - NS data grid only
DNT_NS_Z	Single-component (z) DNT data - NS grid
EM61_3D_XYZ	3-Component EM61-3D Data Set
EM61_3D_Z	Single-component (z) EM61-3D Data Set

The data sets that we described above have been subjected to identical pre-interpretation data processing including the removal of a background response estimated from transients measured over non-anomalous areas of the Blossom Point test site. The net effect is that we have available a set of 3

residual transients at each measurement point falling within a prescribed distance of a target point. In the case of the DNT data, the number of stations varies according to line density and the sample density along line. For the DNT system, one can get a sense of the sample density over an anomaly from the detailed map for target B14 in Figure 1. Those maps show that approximately 75-100 data points fall within a radius of 1.5m from the target center. By construction, the EM61-3D station template required that a total of 74 stations be occupied. The maps in Figures 1 and 3 depict the response for a single component (z) summed over several transient gates. However, the reader must keep in mind that each anomaly has associated with it on the order of 70-100 data points each with the transient data (i.e., 31 gates – DNT & 20 gates – EM61-3D) associated with 3 orthogonal receiver antennas. These data are used to estimate parameters (i.e., position, attitude angles, and 3 polarizability transients) associated with an anisotropic dipole model. The model has been broadly employed throughout the UXO community and will not be described here [8]. The dipole modeling software employed was developed independently by Blackhawk GeoServices [9] and Zonge Engineering [10] closely parallel ideas and methods published by Pasion and Oldenburg [11].

Target Depth Estimations

Grimm [4] based his conclusions on interpretation methods applied to parameters computed with a dipole modeling program developed independently from that used for the bulk of the data processing shown here. So it is important to gain some sense of confidence that the two programs generally produce the same results when applied to the same data set. An important component in the generation of usable target parameters is the correct estimation of target position. Therefore, as one step in our comparison, we have compared the depth estimates provided from various data sets. Figure 5 summarizes the quality of the depth estimates in the form of an overall RMS depth error. The horizontal axis of the figure shows the names of the various data sets. We have sorted the data sets according to increasing depth error. The second (maroon) bar in the graph gives results for a dipole model ("Spheroid Model") that has been constrained to have a single axis of symmetry. The blue bars indicate errors corresponding to the fully unconstrained ("Ellipsoid") model. Grimm's dipole model results ("EM61-3D_XYZ_Grimm") were available for only the ellipsoid model. We make the following observations relative to these results:

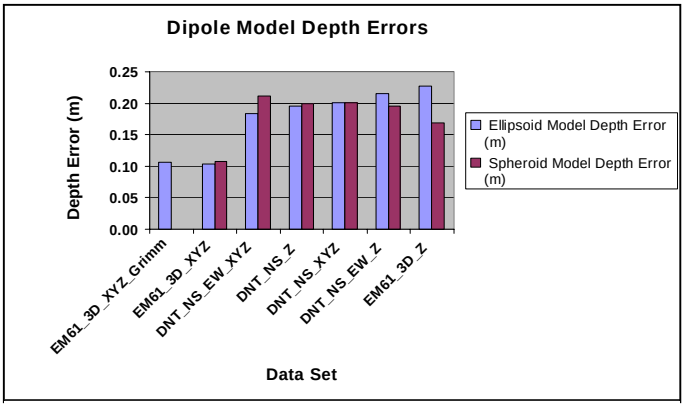

Figure 5: Comparison of dipole model depth errors for Blossom Point data sets.

1. The depth errors indicated by the first 2 data sets ("EM61_3D_XYZ_Grimm" and EM61_3D_XYZ) represent the same data sets processed using two different programs. The fact that the depth errors are approximately the same may be taken as evidence that the Grimm dipole model program and Zonge's DNTDipole produce similar results. The two results indicate that we are estimating target depth with an expected error of about 10cm.
2. Within the DNT data sets, it is significant that we see little or no difference between depth error estimates made with all three components (XYZ) and with a single vertical (Z) components. (see [DNT_NS_EW_XYZ | DNT_NS_EW_Z] and [DNT_NS_XYZ | DNT_NS_Z] in Figure 4.) This suggests that the horizontal components provide little or no added value to quantitative interpretations.

3. It is clear from the difference between the expected depth errors (~10cm) that we obtain with static data (EM61-3D_XYZ) versus the expected errors (~20cm) from the dynamic data, that statically acquired data produces significantly better depth estimates.
4. Finally, note that the expected depth errors for the EM61_3D_Z data sets are slightly larger than those of the DNT data. This seems to suggest that the principal reason for the improved depth estimates in the static data is the horizontal components.

Pasion-Oldenburg Parameters

The final step in the target parameterization using the anisotropic model is to fit the 3 principal polarizability transients (i.e., dPx/dt, dPy/dt, and dPz/dt) with a non-linear function of time and 4 parameters. The use of this function first appeared in a paper by Pasion and Oldenburg [12] [11]. However, they attribute the idea to Duncan McNeill, then president of Geonics. The parametric function is:

$$\frac{dP}{dt} = k\left(t+a\right)^{-b} e^{-ct} \tag{1a}$$

Those readers who have occasion to refer to Grimm's paper [4] will find that he used the same relation with different variable names. Grimm used the relation

$$\frac{dP}{dt} = \beta\left(t+\delta\right)^{-\gamma} e^{-\alpha t} \tag{1b}$$

Our classification algorithms are based on analyses of the 12 parameters that we derive from fitting the three principal polarizability transient curves with equation 1a. In addition, the Zonge parameterization computes the following polarizability moments:

$$P_{0i} = \int_0^\infty \frac{dP_i}{dt} dt \; ; 1 \le i \le 3 \tag{2}$$

$$P_{1i} = \int_0^\infty t \frac{dP_i}{dt} dt \; ; 1 \le \mathrm{i} \le 3 \tag{3}$$

We refer the reader to the paper by Smith and Lee [13] for a discussion of the usefulness of these moments. These moments are easy to calculate and we have found them to be robust classification parameters. Parameters are sorted so that the first parameter (e.g., P_{11}) corresponds to the axis of symmetry in the spheroid model. In the unconstrained models, the 1-axis (i.e., target fixed x-axis) corresponds to the axis with the maximum polarizability value (P_0).

Figure 6 summarizes the parameterization of the EM61-3D data set. In these plots, we mostly use the results we obtain from a spheroid model wherein we constrain the target to have a single axis of symmetry. The upper row of the figures contains plots containing parameters unique to the Zonge software. In the lower row, we plot the Pasion-Oldenburg parameters as used in equation 1a. Note that the plot titled ***Ellipsoid Model Eccentricity*** provides an indication of how well the spheroid model fits the data as compared with an ellipsoidal model. The parameter ***ftest*** takes a value of 1 when the two models fit the data equally well. The parameter P1 Eccentricity is a polarizability ratio formed from the first moment for the fully unconstrained model according to the relation

$$P_{1e} = \frac{\left(P_{12} + P_{13}\right)}{P_{11}} \tag{4}$$

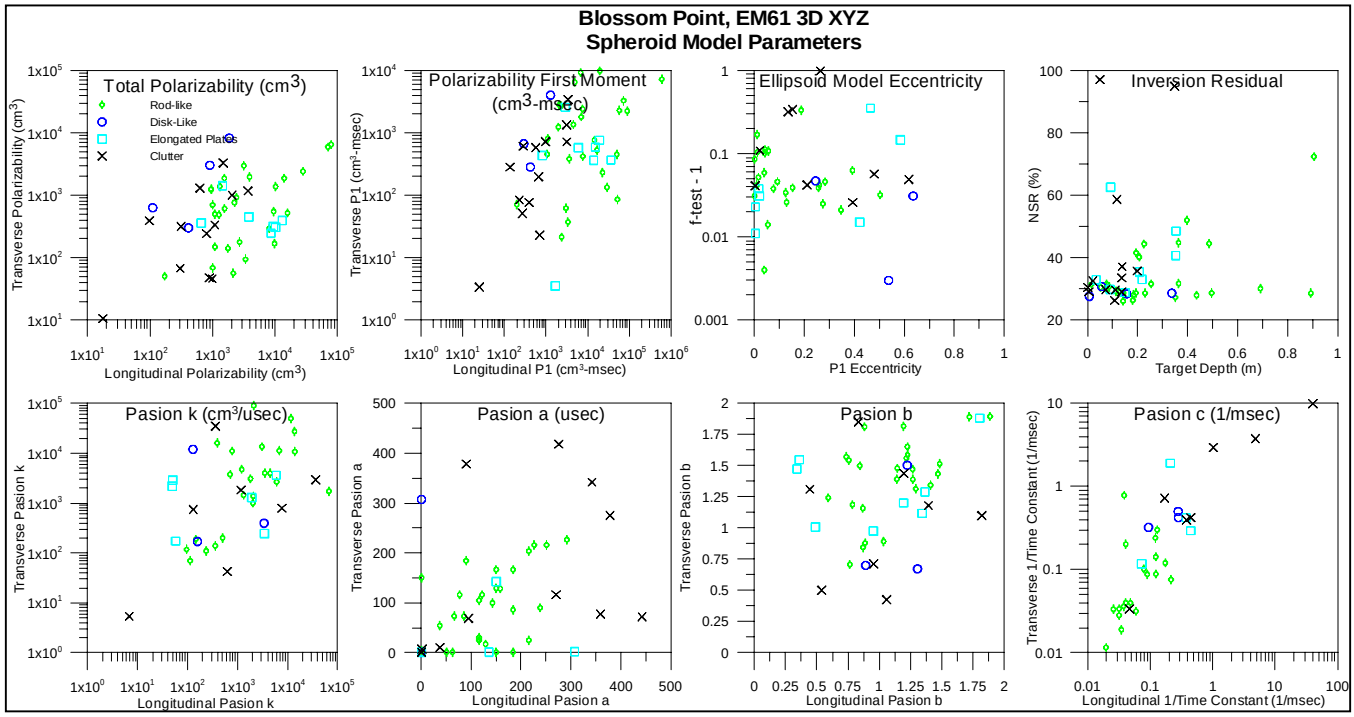

Figure 6: Summary scatter plot for the EM61-3D target parameterization at Blossom Point.

In the ***Ellipsoid Model Eccentricity*** plot, small values of the parameter ***ftest-1*** indicate that the body has an axis of symmetry. Small values of the parameter ***P1 Eccentricity*** (equation 4) indicate that the body is elongated (i.e., a preferred axis for polarization).

Classification

We have experimented with a variety of target ***Classifiers*** during the course of our ESTCP- and SERDP-funded projects. Following the lead of Grimm [4], we apply these classifiers on different data sets defined in Table 1. We use the resulting discrimination ROC curve as a basis for assigning relative merit to the data sets and/or the receiver antenna configuration (i.e., 3-component receiver versus 1-component receiver).

Strong Form Axisymmetry – Grimm noted "excellent" separation between UXO and UXO-like targets at Blossom Point exhibited in the Pasion *b* parameter (Grimm's γ). Grimm used the transverse values of Pasion *b* (b_2 and b_3) as the basis for his so-called "***strong form shape classifier***". In Figure 7, we show ROC curves the EM61-3D data sets based on the strong form shape classifier

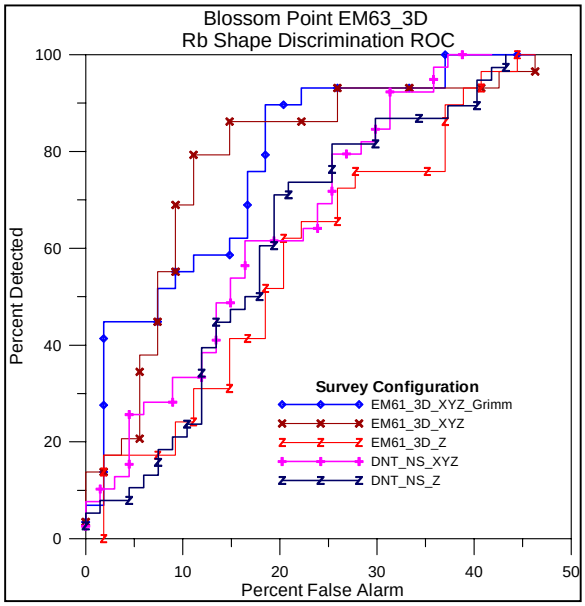

Figure 7: ROC curves for the strong form shape classifier given in equation 5.

$$R_b = 1 - \left(\frac{b_2 - b_3}{b_2 + b_3} \right)^2 \; ; 0 \le R_b \le 1 \qquad (5)$$

These curves are particularly relevant since they show that the classifier produces similar ROC curves for dipole parameters generated by Grimm [4] (blue) and those generated by Zonge's DNTDipole (ochre) for the EM61_3D_XYZ data set. The red curve, derived from EM61_3D_Z, shows that the loss of the horizontal components significantly degrades the performance of the EM61_3D data. We have included ROC curves for 3-component DNT data (magenta) and single-component DNT data (navy blue). Unlike the EM61-3D data, there is very little difference between the performance indicated by the 3-component and single-component DNT data.

Consistent with results reported by Grimm, when we apply the classifier to parameters generated from the EM61_3D_Z data set (red, z-component only), there is a significant decrease in the classification performance compared with full data set. We can therefore be more confident that the results and conclusions that we present here are consistent with those of Grimm.

Table 2: Shape-based discriminant weights based on the analysis of Blossom Point DNT data.

Shape-Based Discrimination Parameters			
Model Parameter	***d1***	***d2***	***d3***
sphere/ellipsoid f-test	-0.0372	0.7245	-0.5974
spheroid/ellipsoid f-test	-0.6297	-0.6295	-0.6801
loop/ellipsoid f-test	0.0009	-0.0904	-0.0167
$\log_{10}$(P0_R)	0.7162	-0.0377	0.4163
P0_E	0.0143	0.0604	0.0028
$\log_{10}$(P1_R)	-0.2886	-0.0683	0.0524
P1_E	-0.0004	-0.0185	-0.0112
PB_1	-0.0600	-0.2226	-0.0584
PB_2	-0.0420	-0.1041	-0.0199
PC_1	0.0178	-0.0157	-0.0180
PC_2	0.0004	0.0013	0.0004

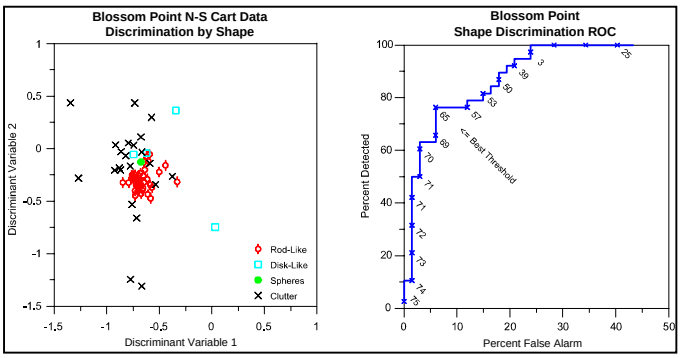

Figure 8: Classification by shape at Blossom Point using LDA. The data set was BP_DNT_XYZ.

Linear Discriminant Analysis (LDA) –Linear discriminant analysis (LDA) has as its objective the prediction of group membership by means of the weighted sum of a set of prediction parameters [14, 15]. Using the scatter plots shown in Figure 6, we analyzed a set of 11 parameters that we believe are good predictors of target shape in order to determine discriminant weights that achieve maximum separation of the targets into 4 groups: rod-like, disk-like, plate-like, and wire loop. The resulting weights for a 3-parameter discriminant function are shown in Table 2. In Figure 8, we show a scatter plot of the values of the discriminants (*d1 & d2*) listed in the table. The scatter plot (left plot) shows that there is excellent separation between rod-like targets and clutter. The ROC curve (right plot) indicates a probability of detection (Pd) of about 78% with a probability of false alarms at approximately 5% when the

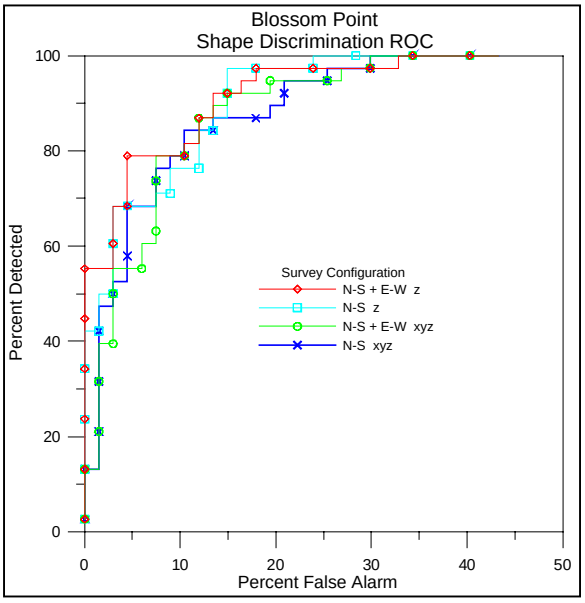

Figure 9: ROC curves representing LDA classification performance on DNT data sets.

threshold is chosen at the indicated point.

Figure 9 is a composite ROC curve that summarizes the performance of this LDA method as applied to the four DNT data sets listed in Table 1. Unlike the ROC curves shown in Figure 7 for static EM61-3D data, the curves in this figure do not indicate that the horizontal components of the dynamically acquired data provide a significant improvement in classification.

Artificial Neural Networks -In addition to the classifiers previously discussed, we have applied two types of artificial neural network classifiers to these data sets:

1. Generalized Regression Neural Networks (GRNN)
2. Conjugate Gradient Neural Networks (CGNN)

GRNN – Grimm [4] implemented a "weak form" classifier based on a GRNN. The 3 multi-gate principal polarizability curves (dPx/dt,dPy/dt,dPz/dt) are reduced to a set of 12 parameters by fitting each transient to the Pasion-Oldenburg relation (equation 1a). Using the resulting 12 Pasion parameters, Grimm forms a set of 8 ratios by normalizing each parameter triplet with the first parameter as shown in equation 6.[2]

$$\mathbf{r}^i = \left\{1, r_2^i, r_3^i\right\} = \left\{1, \frac{p_2^i}{p_1}, \frac{p_3^i}{p_1}\right\};\ \text{where } p_j^i = \left\{k_j, a_j, b_j, c_j\right\}_{1\le j\le 3} \tag{6}$$

The ratio parameters thus defined are insensitive to target size. However, Grimm notes that the resulting ratios, particularly those for Pasion *k* and *b* parameters, are good shape-based target classification parameters. A long axisymmetric target is suggested when the ratios in equation 6 obey the relation $\left(r_2^i \approx r_3^i\right) < 1$. The ROC curves in Figure 10 attributed to Grimm are based on the application of the "weak form" GRNN classification using Pasion parameter ratios.

CGNN-We have developed a multi-layer perceptron neural network architecture with a combination of backpropagation and conjugate gradient learning as an alternative method for classifying UXO. We performed histogram and PCA analyses on 30 parameters from the dipole parameterization (discarding the 3 dP/dt transients and all parameters related to target attitude and position). Based on these analyses, we reduced the number of input parameter to 14.

In Figure 10, we show ROC curves resulting from the application of the CGNN classifier to various data sets. We used 55 measurements from Blossom Point for training and 12 for testing. No measurements from other surveys were used for testing. These curves indicate a dramatic improvement in classification performance between the CGNN classifier and the "strong-form" form shape classifier in Figure 7 and the LDA shape classifier in Figure 8 when these algorithms are applied to DNT

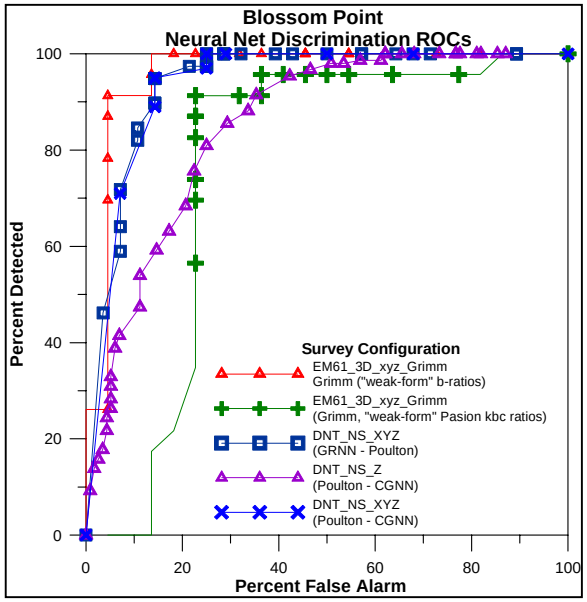

Figure 10: Comparative ROC curves for neural net classification algorithms.

[2]The principal axes are ordered so that the 1-axis is the reference axis. It is generally chosen to correspond with the axis with the maximum response by some measure (e.g., in some specified time gate such as the EM61 gate). When we deal with multi-gate transient responses, as we do here, the choice of the 1-axis may be ambiguous depending on how it is selected.

data. More importantly, however, is that the fact that classification performance is improved when CGNN is applied on 3-component data (blue curve in Figure 10) compared with the performance when it is applied to single (Z) component data (violet curve in Figure 10). This improvement in relative performance on the dynamically acquired DNT data was a pleasant surprise in as much as some of us had worked very hard to demonstrate the "added value" of horizontal components in the DNT data set only to conclude that there was none [5]. These latest results are consistent with those of Grimm and, obviously, more to our liking.

Conclusions

The availability of dynamic and static data sets over targets at the NRL Baseline Ordnance Classification Test Site at Blossom Point has provided us with a rare opportunity to study the performance of multi-gate multi-component TEM systems on several levels. The Geonics EM61-3D data were acquired statically while the Zonge DNT data were acquired dynamically. With the static data, Grimm [4] has demonstrated that a significant improvement in classification is achieved with the acquisition of 3-component data as opposed to a single (vertical) component. Results from re-processing and interpreting Grimm's data with the Zonge processing software support Grimm's conclusions. In our original analyses, those of us associated with Zonge were unable to extend Grimm's conclusions to the dynamically acquired DNT data set. We cited errors in position and attitude associated with dynamic data acquisition with cart-mounted antenna systems together with the relatively higher background EMI noise levels observed in the horizontal components as the most likely source of this degradation in performance. Degradation of model-based classification in general when comparing statically acquired and dynamically acquired data has been noted by Barrow and Nelson [16].

Our noise analysis shows that the noise level in the static EM61-3D is approximately 40dB lower than in the dynamic DNT system. Half of this difference can be accounted for in the EM61-3D by the 15-sec stacking period (~112 base period cycles) employed during the acquisition of the EM61 data. The rest of the background EMI noise (~20dB) in the DNT system is attributed to cart motion. But we have also noted that the behavior of the DNT noise suggests that there is a source of coherent internal (instrument) noise in the Zonge GDP-32^{II}.on one channel.[3] We can expect, and indeed may have already realized, minor improvements in the SNR of the DNT due to reducing or eliminating instrument noise.

We have judged the relative performance between the two instrument systems firstly by comparing the errors in the predicted depths to the targets. As shown in Figure 5, the RMS error in target depth estimates is reduced by a factor of 2 when using static data. Improved estimates in target position translate directly into improvements in the estimation of the polarizability tensor and subsequent Pasion parameters [2].

We have been able to assemble only a single set of ROC curves showing the relative performance of both the static EM61-3D and dynamic DNT systems based on a common classifier (Figure 7). The ROC curves in Figure 7 show that multi-component measurements benefit classification when available in static measurements while they provide no added value in the Zonge DNT system. The performance of the DNT based on the LDA classifier is better than it is for Grimm's ***strong-form shape classifier***. But that is the result of a more sophisticated classifier. Figure 9 confirms what we see in Figure 7 for the DNT system, namely that there is no clear benefit in classification from the 3-component system. It is clear to us that static measurements benefit from both improved SNR from

[3] There have been a number of improvements in the Zonge DNT system hardware and software since Dec. 2001 when the Blossom Point data were acquired and the behavior of the noise on all three channels is more consistent with the predicted $1/\sqrt{t}$ fall off with channel number.

synchronous stacking and greatly reduced antenna position errors resulting from the ability to precisely position the antenna prior to taking a measurement. However, we are very encouraged by the classification performance resulting from using the more advanced CGNN classifier in Figure 10. These results, if they can be reproduced with other data sets, support both the experimentally derived conclusions of Grimm [4] and those of Smith, et. al. [2] based on numerical modeling. We believe, therefore, that measurements of instantaneous position and attitude of the antenna array will provide us with further improvements in discrimination performance using dynamically acquired EMI survey data. But it is equally certain that classification performance from static EMI data will always be better than from dynamic data because position and attitude errors can be virtually eliminated and noise levels can be greatly reduced through signal processing.

Acknowledgements

This work has been supported by contracts with the Environmental Security Technology Certification Program (ESTCP) and the Strategic Environmental Research and Development Program (SERDP).

References

1. Smith, J.T., and H. Frank Morrison, *Estimating Equivalent Dipole Polarizabilities for the Inductive Response of Isolated Conductive Bodies.* submitted to IEEE Trans. Geosci. Remote Sensing, 2002.
2. Smith, J.T., H. Frank Morrison, and Alex Becker, *Resolution Depths for Some Transmitter Receiver Configurations.* submitted to IEEE Trans. Geosci. Remote Sensing, 2002.
3. Smith, J.T., H. Frank Morrison, and Alex Becker, *Optimizing Receiver Configuration for Resolution of Equivalent Dipole Polarizabilities In Situ.* Submitted to Geophysical Research Letters, 2003.
4. Grimm, R.E., *Triaxial Modeling and Target Classification of Multichannel, Multicomponent EM Data for UXO Discrimination.* Jour. Environ. & Eng. Geophys., 2003. **Submitted**: p. 29.
5. Snyder, D.D., Scott C. MacInnes, and Jennifer L. Hare, *A Fast 4-D TEM System for UXO Characterization*. 2003, Zonge Engineering & Research Org., Inc: Tucson, AZ.
6. Nelson, H.H., J.R. McDonald, and Richard Robertson, *Design and Construction of the NRL Baseline Ordnance Classification Test Site at Blossom Point*. 2000, Naval Research Laboratory: Washington, DC. p. 13.
7. Nelson, H.H., T.H. Bell, J.R. McDonald, and B. Barrow, *Advanced MTADS Classification for Detection and Discrimination of UXO*. 2003, Naval Research Laboratory: Washington, D.C. p. 53.
8. Barrow, B., and H. H. Nelson, *Model-Based Characterization of Electromagnetic Inudction Signatures Obtained with the MTADS Electromagnetic Array.* IEEE Trans Geosci & Rem. Sensing, 2001. **39**(6): p. 1279-1285.
9. Grimm, R.E., and T.A. Sprott. *Model-based sensor design optimization for UXO classification*. in *UXO/Countermine Forum 2002*. 2002. Orlando, FL: U.S. Dept of Defense Explosives Safety Board.
10. MacInnes, S.C., Donald D. Snyder, and Kenneth L. Zonge. *Physics-Based Characterization of UXO from Multi-Component TEM Data*. in *UXO/Countermine Forum*. 2002. Orlando, FL: U.S. Dept. of Defense.
11. Pasion, L.R., and D.W. Oldenburg, *A Discrimination Algorithm for UXO Using Time Domain Electromagnetics.* Jour. Eng. & Envir. Geophys., 2001(28): p. 91-102.
12. Pasion, L.R., and Douglas W. Oldenburg. *Locating and Determining Dimensionality of UXOs Using Time Domain Electromagnetic Induction*. in *SAGEEP 1999*. 1999. Oakland, CA.

13. Smith, R.S., and Terry J. Lee, *The moments of the impulse response: A new paradigm for the interpretation of transient electromagnetic data.* Geophysics, 2002. **67**(4): p. 1095-1103.
14. Hastie, T., Robert Tibshirana, and Jerome Friedman, *The Elements of Statistical Learning - Data Mining, Inference, and Prediction*. Springer Series in Statistics. 2001, New York: Springer. 533.
15. Tabachnick, B.G., and Linda S. Fidell, *Using Multivariate Statistics*. 2nd ed. 2001, Boston: Allyn & Bacon. 966.
16. Barrow, B., and Herbert H. Nelson. *Effects of Position Error on Inverting EMI Data for UXO Discrimination Using the MTADS Platform*. in *The UXO/Countermine Forum*. 2001. New Orleans, LA: U.S. Dept. of Defense.